Zeolite Structures

DOI: 10.1002/ange.200501939

Structure Elucidation of the Highly Active Titanosilicate Catalyst Ti-YNU-1**

*Juanfang Ruan, Peng Wu, Ben Slater, and Osamu Terasaki**

A major breakthrough in the field of zeolite catalysis was the development of MFI-type (a zeolite framework type of ZSM-5) titanosilicate (TS-1) as a liquid-phase oxidation catalyst.[1] Nevertheless, TS-1 has a major disadvantage in that its medium-sized pores with 10-membered rings (10-MRs) restrict its application to molecules of relatively small size. To overcome this problem of TS-1, other titanosilicates with larger pores, such as Ti-Beta,[2,3] Ti-MOR,[4] Ti-ITQ-7,[5] and Ti-MCM-41,[6] have been prepared and have partially solved the problems of steric constraints encountered in the oxidation of bulky molecules. However, it seems that none of the above titanosilicates has sufficient intrinsic activity and stability, and this has stimulated researchers to prepare Ti-containing catalysts that are both highly stable and accessible to bulky substrates. In this context, MWW-type zeolite has a promising framework structure consisting of MWW sheets and contains two independent noninterconnected pore systems with 10-MR channels.[7,8] Three-dimentional (3D) Ti-MWW was successfully prepared by hydrothermal synthesis,[9] but on calcination of the layered MWW sheets, access to the supercages is seriously restricted by the openings of the 10-MR pores. Thus, in the case of aluminosilicate, a micro-mesoporous hybrid material MCM-36 was prepared by swelling the MWW sheets of the lamellar precursor with organic surfactant followed by pillaring with a silica precursor.[10] With similar objectives, ITQ-2 was synthesized by swelling the layers of the MWW lamellar precursor and than sonicating the product.[11] Both MCM-36 and ITQ-2 have an extremely high surface area that is highly accessible to bulky molecules, but lack an ordered crystalline structure. From a steric point of view, it is desirable to retain the space between the MWW sheets after calcining the lamellar precursor. In the particular case of the titanosilicate, this not only makes the active sites within the supercages more accessible to bulky molecules, but also promotes activity in oxidation reactions with aqueous H_2O_2 as oxidant, as the silanol groups are less hydrophilic than in pillared and delaminated materials. This could open up new applications for titanosilicates in the synthesis of fine chemicals. Previously, a novel titanosilicate denoted Ti-YNU-1 was prepared from an MWW-type precursor.[12] It has an expanded pore window between the crystalline MWW sheets and shows a far higher intrinsic catalytic activity than 3D Ti-MWW and large-pore Ti-Beta in the epoxidation of bulky alkenes with H_2O_2. Although Ti-YNU-1 was reported to contain MWW sheets, the nature and structure of the linkage between the sheets were not established. We have now investigated the structure of Ti-YNU-1 by focusing on the pore structure and space between the MWW sheets at the atomic scale by high-resolution transmission electron microscopy (HRTEM), powder X-ray diffraction (XRD), scanning electron microscopy (SEM), and NMR spectroscopy. From a combination of computer simulations and experimental observations, we suggest a likely structure of Ti-YNU-1.

The SEM images of the MWW lamellar precursor, 3D Ti-MWW, and Ti-YNU-1 samples are shown in Figure 1. All samples crystallized as thin platelets with hexagonal morphology, and the unit cell *c* axis lies perpendicular to the plate surface. The thin platelets of all samples were approximately 2 μm in width and 0.1 μm in thickness; no significant differences in morphology between the three samples can be discerned from the images, although some roughening of the crystal edges in the Ti-YNU-1 sample is evident.

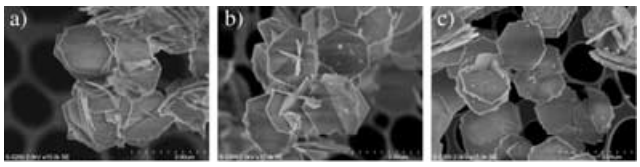

Figure 1. SEM images of a) lamellar precursor, b) 3D Ti-MWW, and c) Ti-YNU-1.

The XRD pattern of the lamellar precursor shows reflections at large scattering angles that are much broader than those of 3D Ti-MWW and Ti-YNU-1 (Figure 2). This indicates that the lamellar precursor is composed of MWW sheets, and on acid treatment or calcination the sheets are fully connected to form 3D Ti-MWW or Ti-YNU-1. The powder XRD pattern of Ti-YNU-1 appears to be similar to those of the lamellar precursor and 3D Ti-MWW, but the principal difference is that the diffraction peaks associated

[*] J. Ruan, Prof. O. Terasaki
Structural Chemistry, Arrhenius Laboratory
Stockholm University
Stockholm, 10691 (Sweden)
Fax: (+46) 8-163-118
E-mail: terasaki@struc.su.se
Prof. P. Wu
Shanghai Key Laboratory of Green Chemistry and Chemical Processes
Department of Chemistry, East China Normal University
North Zhongshan Rd. 3663, Shanghai, 200062 (China)
Dr. B. Slater
Davy Faraday Research Laboratory
The Royal Institution of Great Britain
21 Albemarle Street, London W1S4BS (UK)

[**] O.T. thanks the Swedish Science Research Council (VR) and the Japan Science and Technology Cooperation (JST) for financial support. P.W. thanks the Program for New Century Excellent Talents in University (NCET), the NSFC (No. 20473027), and Prof. T. Tatsumi for his encouragement. B.S. thanks Prof. Julian D. Gale and Prof. Javier Junquera for basis and pseudopotential data for SIESTA, and the EPSRC for computing time on the HPC(x) UK national supercomputer facility.

Supporting information for this article is available on the WWW under http://www.angewandte.org or from the author.

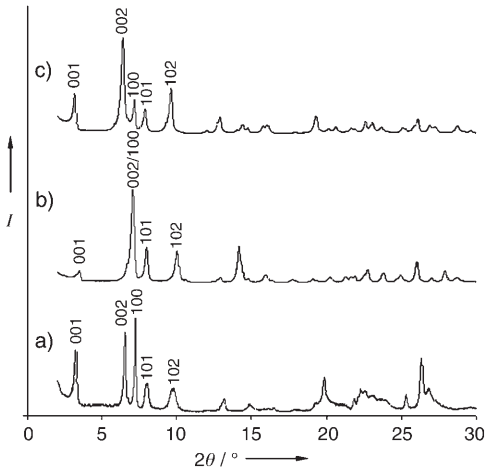

Figure 2. Powder XRD profiles of a) lamellar precursor, b) 3D Ti-MWW, and c) Ti-YNU-1.

with unit-cell distance c are all shifted to lower 2θ values in comparison to the lamellar precursor and 3D Ti-MWW. For example, the (001) peak of Ti-YNU-1 is found at 3.20°, (002) at 6.41°, and (101) at 7.85°, but for 3D Ti-MWW and the lamellar precursor, (001) is found at 3.52° and 3.29°, (002) at 7.04° and 6.56°, and (101) at 7.97° and 7.94°. In contrast, the diffraction peaks associated with unit-cell distance a remain almost constant: (100) is found at 7.16°, as opposed to 7.15° and 7.23° for 3D Ti-MWW and the lamellar precursor, respectively. These observations suggest that calcination and acid treatment do not affect the basic crystalline structure within the layers, but do influence the space between the MWW sheets. Table 1 lists the powder XRD data of the lamellar precursor, 3D Ti-MWW, and Ti-YNU-1. The unit-cell parameters were calculated to be $a=b=$ 14.238 Å and $c=27.571$ Å for Ti-YNU-1, $a=b=14.263$ Å and $c=$ 25.098 Å for 3D Ti-MWW, and $a=b=14.108$ Å and $c=26.926$ Å for the lamellar precursor. The parameter c of Ti-YNU-1 is enlarged by about 2.5 and 0.6 Å relative to those of 3D Ti-MWW and the lamellar precursor, respectively. The structural expansion also led to an enlarged specific surface area and pore volume for Ti-YNU-1 (654 $m^2 g^{-1}$ and 0.20 $mL g^{-1}$) in comparison to 3D Ti-MWW (548 $m^2 g^{-1}$ and 0.16 $mL g^{-1}$; see Supporting Information).

Table 1: Powder XRD data of lamellar precursor, 3D Ti-MWW, and Ti-YNU-1.

Lamellar precursor			3D Ti-MWW			Ti-YNU-1		
hkl	2θ [°]	d_{hkl} [Å]	*hkl*	2θ [°]	d_{hkl} [Å]	*hkl*	2θ [°]	d_{hkl} [Å]
001	3.29	26.926	001	3.52	25.089	001	3.20	27.571
002	6.56	13.463	002	7.04	12.544	002	6.41	13.786
100	7.23	12.218	100	7.15	12.352	100	7.16	12.331
101	7.94	11.126	101	7.97	11.082	101	7.85	11.257
102	9.77	9.047	102	10.04	8.801	102	9.62	9.191
003	9.85	8.975	003	10.57	8.363	003	9.62	9.191
103	12.23	7.233	103	12.77	6.925	103	12.00	7.369
111	12.96	6.824	111	12.89	6.860	111	12.83	6.893
004	13.14	6.731	004	14.11	6.272	004	12.83	6.893
112	14.16	6.248	112	14.27	6.200	112	13.99	6.326
200	14.49	6.109	200	14.33	6.176	200	14.35	6.166
201	14.86	5.957	201	14.76	5.997	201	14.71	6.017
104	15.01	5.896	104	15.83	5.593	104	14.71	6.017
202	15.92	5.563	202	15.98	5.541	202	15.73	5.628
113	15.97	5.546	113	16.32	5.426	113	15.73	5.628
005	16.45	5.385	005	17.66	5.018	005	16.06	5.514
203	17.55	5.050	203	17.84	4.968	203	17.30	5.120
105	17.99	4.928	210	18.99	4.669	105	19.03	4.661
210	19.20	4.618	105	19.08	4.649	210	19.03	4.661
211	19.49	4.551	211	19.32	4.590	211	19.30	4.596
204	19.61	4.524	204	20.16	4.401	204	19.30	4.596
006	19.77	4.488	212	20.28	4.375	006	19.30	4.595
212	20.31	4.368	006	21.23	4.181	212	20.09	4.415
115	20.73	4.280	300	21.57	4.117	115	20.35	4.360
106	21.07	4.212	115	21.64	4.104	106	20.61	4.306
213	21.62	4.106	213	21.78	4.076	213	21.36	4.157
300	21.81	4.073	301	21.86	4.063	300	21.60	4.111

The [001] HRTEM images of the lamellar precursor, 3D Ti-MWW, and Ti-YNU-1 are shown in Figure 3 together with corresponding Fourier diffractograms (FDs). The image and FD of Ti-YNU-1 show no significant differences from those of the lamellar precursor and 3D Ti-MWW, which clearly exhibit the characteristic hexagonal framework topology of MWW-type materials in this projection.[7] It is apparent that postprocessing does not alter the structure within the MWW sheet, and there is no evidence for aperiodically or periodically repeating defects. As all three materials show the same projected images of the MWW sheet (and the same FDs), structural study of Ti-YNU-1 perpendicular to the MWW sheet, that is, along [100], is essential to find differences between the lamellar precursor, 3D Ti-MWW, and Ti-YNU-1.

The HRTEM images of the lamellar precursor, 3D Ti-MWW, and Ti-YNU-1 with [100] incidence and the corresponding FDs are shown in Figure 4. The image of the lamellar precursor was taken under overfocus conditions and indicates the presence of 3D order (Figure 4a). The image of Ti-YNU-1 in Figure 4c was taken under underfocus conditions and reveals that it has a structure similar to that 3D Ti-MWW (Figure 4b) but with a different c distance. Selected-area electron diffraction with the calibration of the camera length was conducted to show the different c distances of Ti-YNU-1 and 3D Ti-MWW (see Supporting Information). To confirm the above observations, HRTEM images for [100] incidence were simulated for both over- and underfocus conditions by the multislice method using the structural parameters of 3D MWW (see Supporting Information). By comparing these simulated images with the observed

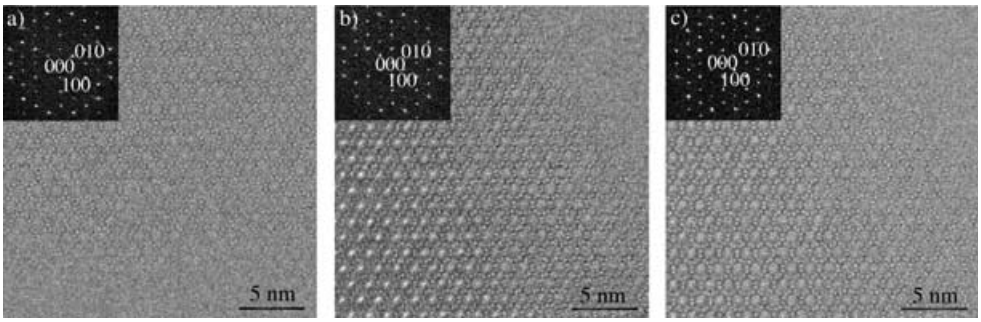

Figure 3. HRTEM images of a) lamellar precursor, b) 3D Ti-MWW, and c) Ti-YNU-1 taken with [001] incidence. Corresponding FDs are inset in each image.

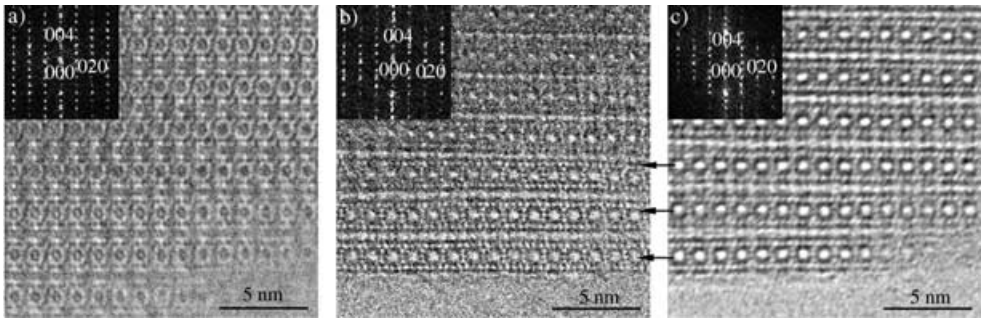

Figure 4. HRTEM images of a) lamellar precursor, b) 3D Ti-MWW, and c) Ti-YNU-1 taken with [100] incidence. Corresponding FDs are inset in each image.

HRTEM images of Figure 4, we conclude that Ti-YNU-1 has a 3D-connected framework structure of the MWW type, analogous to that of 3D Ti-MWW. On the other hand, the lamellar precursor also has a 3D ordered structure, which indicates that the structure-directing agent present in the interlayer region causes regular stacking along *c* at a well-defined distance.

To further probe the nature of the interlayer structure in Ti-YNU-1, ^{29}Si MAS (magic-angle spinning) NMR spectroscopy was performed. The spectrum of Ti-YNU-1 (Figure 5) showed a Q^2 band around 89 ppm which was absent for 3D Ti-MWW. This band implies the possible presence of $Si(OH)_2(SiO_2)_2$ or $Si(OH)(OTi)(SiO_2)_2$ linkages between the MWW sheets. Considering that Ti-YNU-1 has a lattice expansion of about 2.5 Å, as confirmed by XRD, wholly intact linkages between MWW layers according to HRTEM observations, and the potential linking species indicated by NMR spectra, it is proposed that the Ti-YNU-1 structure is simply an expanded form of MWW in which a single T site acts as a pillar connecting the MWW layers (Figure 6).

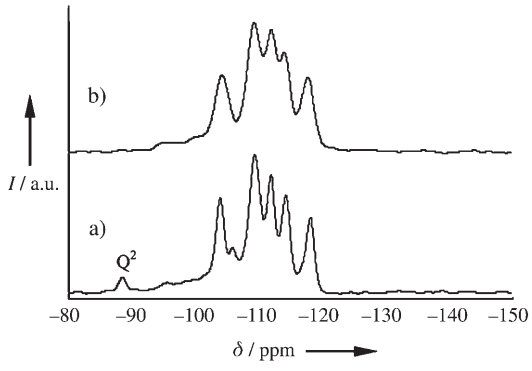

Figure 5. ^{29}Si MAS NMR spectra of a) Ti-YNU-1 and b) 3D Ti-MWW.

Atomistic computer simulation techniques were used to model the proposed crystal structure. Initially, we used methods based on interatomic potentials, as described by, for example, Chiu et al.[13] and Jentys and Catlow,[14] to verify the bulk structure of pure Si-MWW, using the GULP code.[15] The computed cell parameters of 14.187, 14.187, and 24.957 Å are within 0.5% of the measured values reported by Corma and co-workers.[16]

To assess potential Ti-YNU-1 structures, we first constructed a model in which two additional T sites are introduced per unit cell, midway between the lamellar layers of MWW, to form layer spacing or $Si(OH)_2$ "pillars". This

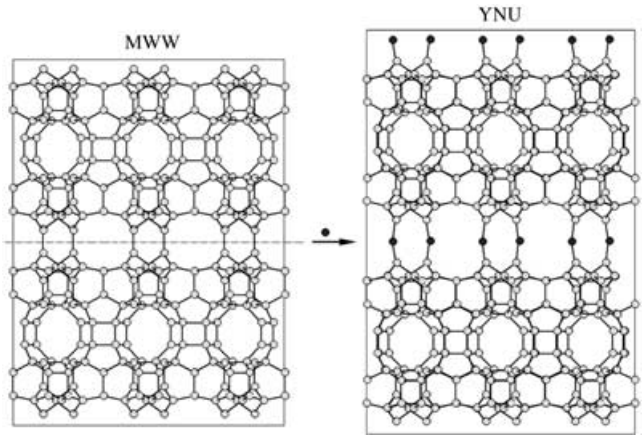

Figure 6. Schematic transformation of MWW to YNU.

structure was then relaxed by using the computational approach outlined above to give the structure shown in Figure 7a. Introduction of two additional T sites causes essentially no change in the *a* and *b* lattice parameters but an expansion in the *c* direction of 2.59 Å relative to pure Si-MWW. This increase closely agrees with the magnitude of the structural expansion inferred from XRD and TEM. Critically, the introduction of the additional T sites expands the

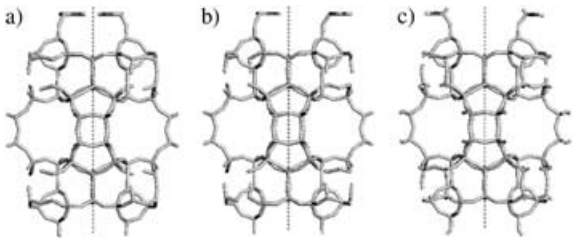

Figure 7. Three possible configurations for Si-YNU indicating the flexible nature of the 12-MR, viewed along [100].

interlayer ten-membered ring to form a twelve-membered ring, which affords increased transport rates and the potential to filter larger products than the 10-MR. Two other possible configurations were generated, one in which the T sites are placed as close together as possible and an "indented 12-MR" configuration (Figure 7b and c). The relative energies of the configurations shown in Figure 7a–c (0.079, 0.084, and 0.000 eV, respectively) are almost identical and are comparable to kT, and this suggests that at moderate temperature, because the $Si(OH)_2$ group can freely rotate, all three of these configurational states will be occupied on a picosecond timescale. The breathing of the 12-MR will lead to electron scattering and hence weak contrast in the HRTEM image.

Finally, the substitution energetics for Ti in MWW was assessed by the interatomic potential approach. The span of Ti substitution energies measured relative to the most favorable site is 0.70 eV for the potentials reported by Jentys and Catlow.[14] The spread of energies is substantially greater than that in silicalite, for which the range is about 0.22 eV, from which it can be inferred that the selectivity of Ti for particular lattice sites within MWW is rather high. As the typical Ti/Si ratio for MWW is about 1:240, it follows that the sixfold rim site shown in Figure 8, which is identified as the lowest energy site, may be selectively occupied. As the next most favorable site is 0.14 eV higher in energy than the rim site, the rim site is likely to be occupied first. In Figure 8, the location of the most (rim) and least (spiro) favorable sites (shown in white and black, respectively) are displayed. However, it is worth noting that the activation barrier for formation of MWW/YNU is likely to be comparable to the range of substitution energies, and hence ordering of Ti towards particular lattice sites may be relaxed due to kinetically favored pathways.

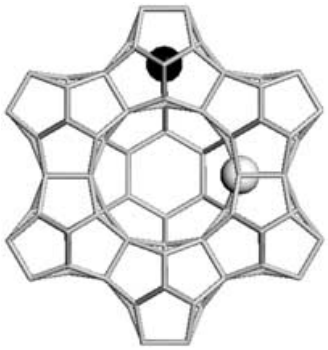

Figure 8. A [001] view of Ti-YNU indicating favorable substitution at the "rim" site (white) and less favorable incorporation at the "spiro" site (black).

To assess the preferred location of framework Ti in Ti-YNU, the proposed Si-YNU structure was first relaxed using the local-orbital-based, periodic density functional code SIESTA.[17] A titanium center was then introduced into the unit cell at the pillar site and at the most and least favorable sites in the MWW sheet, identified by the interatomic potential calculations, to give three distinct configurations that were relaxed at constant pressure. The relative stability of the three sites was rim > pillar > spiro, with relative energies of 0, +0.24, +0.27 eV, respectively, under anhydrous conditions. Although the pillar site appears not to be the most favorable framework site, the position of Ti within the YNU lattice will depend strongly on the water content[18] in the lattice and on the susceptibility to Ti leaching from MWW lamellae under acid conditions. It is possible that under acid/reflux conditions, Ti would leach from the rim site and occupy the pillar site, where it could easily expand its coordination sphere to give a quasi-octahedral configuration. In the pillar site, Ti could easily physisorb one or more water molecules and thus enhance its stability within the lattice while retaining steric accessibility and a flexible coordination number for catalytic activity.

The simulated XRD pattern of the proposed Ti-YNU-1 structure compares well with measured data (see Supporting Information). The HRTEM images simulated for the new structure with 12-MRs match very favorably with the observed images (see Supporting Information). However the differences between the images of MWW 10-MRs and Ti-YNU-1 12-MRs are extremely slight, except for the marked increase in c. The weight of evidence suggests that Ti-YNU-1 has 12-MRs between the MWW sheets from the observed c period in the HRTEM image and the XRD data.

In conclusion, the structure of Ti-YNU-1, which is structurally related to MWW, was studied by TEM in combination with powder XRD, SEM, NMR spectroscopy, and computer simulations. We found that Ti-YNU-1 has a 3D-connected MWW-like framework with much larger spacing along the c axis between the MWW sheets than the lamellar precursor and 3D Ti-MWW. A newly formed 12-MR that is distinct from the 10-MR of the MWW structure would explain this cell expansion. The expanded pore window, which would result in a concomitant increase in steric accessibility, may explain the significant enhancement of catalytic activity measured relative to other titanosilicates. Additionally, simulation results suggest that Ti has high site selectivity relative to materials such as MFI,[18] and we speculate that the Ti centers could occupy the pillar sites, which have a much higher steric accessibility than framework positions in MWW and, for example, TS-1. It is tempting to speculate that Ti in the pillar site of YNU will be conducive to temporary expansion of the Ti coordination sphere, which is thought to be crucial to epoxidation activity in, for example, TS-1.[19] As the silicon or titanium ions that intercalate the sheets must originate from the framework by acid treatment, an intriguing possibility would be to adjust the postsynthesis procedure to include silicate monomers or larger oligomers, and thus to potentially design the pillar height and hence ring size. Such

an approach could lead to tailored zeolites with the capability to obtain extremely high selectivity.

Experimental Section

The lamellar precursor of the MWW titanosilicate was synthesized from highly siliceous MWW zeolite, tetrabutyl orthotitanite (TBOT), piperidine (PI), and deionized water following procedures reported elsewhere.[12] Typically, PI (7.24 g) and TBOT (0.29 g) were dissolved in 22.5 g of deionized water, then a highly deboronated MWW (5 g) was added to the solution. The resultant mixture was rotated in an autoclave at 443 K for 5 days. The as-synthesized precursor (Si/Ti = 100, containing 15.4 wt % PI) was directly calcined at 823 K for 10 h to burn off PI and obtain the 3D MWW titanosilicate Ti-MWW (Si/Ti = 100). This was heated at reflux in 2 M HNO_3 solution and further calcined at 823 K for 10 h to obtain a novel titanosilicate, denoted Ti-YNU-1 (Si/Ti = 240).

Powder X-ray diffraction (XRD) patterns were collected on a MAC Science MX-Labo diffractometer ($Cu_{K\alpha}$ radiation). The crystal size and morphology were monitored by SEM on a Hitachi S-5200 microscope. For TEM measurements, the sample was crushed in an agate mortar, dispersed in ethanol (95 vol %) by ultrasonication, and then dropped onto a carbon microgrid. HRTEM observations were carried out with a 300 kV TEM (JEOL-3010, $C_s = 0.6$ mm, resolution 1.7 Å). Images were recorded with a Kodak electron film SO-163 using low-electron-dose conditions. The HRTEM images were simulated by the multslice method using the MacTempas program as a function of crystal thickness and defocus values under the parameters of an accelerated voltage of 300 kV, $C_s = 0.6$ mm, and semiangle of beam convergence of 0.6 mrad. The ^{29}Si MAS NMR spectra were recorded on a JEOL ECA-400 multinuclear solid-state magnetic resonance spectrometer at 79.6 MHz at a spinning rate of 5 kHz and with a pulse interval of 15 s.

Received: June 4, 2005
Revised: July 14, 2005
Published online: September 19, 2005

Keywords: layered compounds · silicates · structure elucidation · titanates · zeolite analogues

[1] G. Bellussi, M. S. Rigutto, *Stud. Surf. Sci. Catal.* **2001**, *137*, 911.
[2] M. A. Camblor, A. Corma, A. Martínez, J. Pérez-Pariente, *J. Chem. Soc. Chem. Commun.* **1992**, 589.
[3] T. Tatsumi, N. Jappar, *J. Phys. Chem. B* **1998**, *102*, 7126.
[4] P. Wu, T. Komatsu, T. Yashima, *J. Phys. Chem.* **1996**, *100*, 10316.
[5] M. Díaz-Cabañas, L. A. Villaescusa, M. A. Camblor, *Chem. Commun.* **2000**, 761.
[6] A. Corma, *Chem. Rev.* **1997**, *97*, 2373.
[7] M. E. Leonowicz, J. A. Lawton, S. L. Lawton, M. K. Rubin, *Science* **1994**, *264*, 1910.
[8] G. G. Juttu, R. F. Lobo, *Microporous Mesoporous Mater.* **2000**, *40*, 9.
[9] P. Wu, T. Tatsumi, T. Komatsu, T. Yashima, *J. Phys. Chem. B* **2001**, *105*, 2897.
[10] W. J. Roth, C. T. Kresge, J. C. Vartuli, M. E. Leonowicz, A. S. Fung, S. B. McCullen, *Stud. Surf. Sci. Catal.* **1995**, *94*, 301.
[11] A. Corma, V. Fornés, S. B. Pergher, Th. L. M. Maesen, J. G. Buglass, *Nature* **1998**, *396*, 353.
[12] W. B. Fan, P. Wu, S. Namba, T. Tatsumi, *Angew. Chem.* **2004**, *116*, 238; *Angew. Chem. Int. Ed.* **2004**, *43*, 236.
[13] M. E. Chiu, B. Slater, J. D. Gale, *Angew. Chem.* **2005**, *117*, 1239; *Angew. Chem. Int. Ed.* **2005**, *44*, 1213.
[14] A. Jentys, C. R. A. Catlow, *Catal. Lett.* **1993**, *22*, 251.
[15] J. D. Gale, A. L. Rohl, *Mol. Simul.* **2003**, *29*, 291.
[16] M. A. Camblor, A. Corma, M. Díaz-Cabañas, C. Baerlocher, *J. Phys. Chem. B* **1998**, *102*, 44.
[17] D. Sanchez-Portal, P. Ordejon, E. Canadell, *Struct. Bonding (Berlin)* **2004**, *113*, 103.
[18] G. Ricchiardi, A. J. M. de Man, J. Sauer, *Phys. Chem. Chem. Phys.* **2000**, *2*, 2195.
[19] M. Neurock, L. E. Manzer, *Chem. Commun.* **1996**, 1133.

